

Effect of Cu doping on the secondary electron yield of carbon films on Ag-plated aluminum alloy

Tiancun Hu(胡天存), Shukai Zhu(朱淑凯), Yanan Zhao(赵亚楠), Xuan Sun(孙璇), Jing Yang(杨晶), Yun He(何鋆), Xinbo Wang(王新波), Chunjiang Bai(白春江), He Bai(白鹤), Huan Wei(魏焕), Meng Cao(曹猛), Zhongqiang Hu(胡忠强), Ming Liu(刘明), and Wanzhao Cui(崔万照)

Citation: Chin. Phys. B, 2022, 31 (**4**): 047901. DOI: 10.1088/1674-1056/ac322c
Journal homepage: http://cpb.iphy.ac.cn; http://iopscience.iop.org/cpb

What follows is a list of articles you may be interested in

Secondary electron emission yield from vertical graphene nanosheets by helicon plasma deposition

Xue-Lian Jin(金雪莲), Pei-Yu Ji(季佩宇), Lan-Jian Zhuge(诸葛兰剑), Xue-Mei Wu(吴雪梅), and Cheng-Gang Jin(金成刚)

Chin. Phys. B, 2022, 31 (**2**): 027901. DOI: 10.1088/1674-1056/ac11dd

Analysis of secondary electron emission using the fractal method

Chun-Jiang Bai(白春江), Tian-Cun Hu(胡天存), Yun He(何鋆), Guang-Hui Miao(苗光辉), Rui Wang(王瑞), Na Zhang(张娜), and Wan-Zhao Cui(崔万照)

Chin. Phys. B, 2021, 30 (**1**): 017901. DOI: 10.1088/1674-1056/abc2be

Secondary electron yield suppression using millimeter-scale pillar array and explanation of the abnormal yield-energy curve

Ming Ye(叶鸣), Peng Feng(冯鹏), Dan Wang(王丹), Bai-Peng Song(宋佰鹏), Yong-Ning He(贺永宁), Wan-Zhao Cui(崔万照)

Chin. Phys. B, 2019, 28 (**7**): 077901. DOI: 10.1088/1674-1056/28/7/077901

A synthetic semi-empirical physical model of secondary electron yield of metals under *E*-beam irradiation

Guo-Bao Feng(封国宝), Wan-Zhao Cui(崔万照), Na Zhang(张娜), Meng Cao(曹猛), Chun-Liang Liu(刘纯亮)

Chin. Phys. B, 2017, 26 (**9**): 097901. DOI: 10.1088/1674-1056/26/9/097901

Formula for average energy required to produce a secondary electron in an insulator

Xie Ai-Gen, Zhan Yu, Gao Zhi-Yong, Wu Hong-Yan

Chin. Phys. B, 2013, 22 (**5**): 057901. DOI: 10.1088/1674-1056/22/5/057901

Effect of Cu doping on the secondary electron yield of carbon films on Ag-plated aluminum alloy

Tiancun Hu(胡天存)[1,2], Shukai Zhu(朱淑凯)[3], Yanan Zhao(赵亚楠)[3,†], Xuan Sun(孙璇)[3], Jing Yang(杨晶)[2], Yun He(何鋆)[2], Xinbo Wang(王新波)[2], Chunjiang Bai(白春江)[2], He Bai(白鹤)[2], Huan Wei(魏焕)[2], Meng Cao(曹猛)[1], Zhongqiang Hu(胡忠强)[3], Ming Liu(刘明)[3], and Wanzhao Cui(崔万照)[2,‡]

[1] *Key Laboratory for Physical Electronics and Devices of the Ministry of Education, School of Electronic Science and Engineering, Xi'an Jiaotong University, Xi'an* 710049, *China*

[2] *National Key laboratory of Science and Technology on Space Microwave, China Academy of Space Technology (Xi'an), Xi'an* 710100, *China*

[3] *Electronic Materials Research Laboratory, Key Laboratory of the Ministry of Education & International Center for Dielectric Research, School of Electronic Science and Engineering, Xi'an Jiaotong University, Xi'an* 710049, *China*

(Received 8 September 2021; revised manuscript received 12 October 2021; accepted manuscript online 22 October 2021)

Reducing the secondary electron yield (SEY) of Ag-plated aluminum alloy is important for high-power microwave components. In this work, Cu doped carbon films are prepared and the secondary electron emission characteristics are studied systematically. The secondary electron coefficient δ_{max} of carbon films increases with the Cu contents increasing at first, and then decreases to 1.53 at a high doping ratio of 0.645. From the viewpoint of surface structure, the higher the content of Cu is, the rougher the surface is, since more cluster particles appear on the surface due to the small solid solubility of Cu in the amorphous carbon network. However, from viewpoint of the electronic structure, the reduction of the sp^2 hybrid bonds will increase the SEY effect as the content of Cu increases, due to the decreasing probability of collision with free electrons. Thus, the two mechanisms would compete and coexist to affect the SEY characteristics in Cu doped carbon films.

Keywords: copper-doped carbon, secondary electron yield, microwave devices, surface roughness

PACS: 79.20.Hx **DOI:** 10.1088/1674-1056/ac322c

1. Introduction

High-power microwave components are one of the core payloads in spacecrafts and satellites.[1–4] However, the multipactor effects become more and more destructive in space as the microwave devices become miniaturized and integrated. The multipactor effects can increase the surface temperature of microwave components and the noise level of the microwave devices which decreases the output power levels.[5,6] In more serious cases, permanent failures of microwave components may occur. Therefore, improving the multipactor threshold of microwave components or avoiding the multipactor has become a key research topic,[7–9] which should be considered in designing satellite systems with high-power microwave components.

Generally, the multipactor effect is strongly related to the secondary electron yield (SEY) of the materials.[10–12] The two most commonly used methods to suppress SEY effects are micro-trapping structure surface[13–17] and surface coating with low SEY materials.[8] Ye *et al.* reduced the maximum secondary electron emission coefficient (δ_{max}) by 60% by fabricating the triangular raised structures.[18] Bai *et al.* prepared porous anodic alumina films with various hole sizes on aluminum alloy substrates,[19] resulting in an obvious inhibiting effect in the SEY coefficient. However, the signal transmission becomes worse and energy loss also increases when the operations are applied to high power microwave devices. He *et al.* sputtered platinum film (100 nm) on the surface of silver plating aluminum alloy samples,[20] in which the maximum SEY coefficient decreased from 2.40 to 1.77. In addition, TiN_2 thin films were prepared on monocrystalline silicon and glass by RF magnetron sputtering,[16] and it not only efficiently suppresses the SEY coefficients but also improves the threshold value of multipactors of components.

The amorphous carbon (C) film[5,7,21–23] is a metastable material with coexistence of diamond phase and graphite phase,[24–27] which could suppress the SEY effect through a simple coating process. Copper metals also have small secondary electron emission coefficients and their electrical conductivities satisfy the requirements of microwave components.[28] In this study, copper doped carbon films are sputtered on silver-plated aluminum alloy substrates. Then, the secondary electron yield characteristics of the C/Cu composite films are systematically analyzed by the x-ray photoelectron spectroscopy and scanning electron microscopy. In addition, sp^2/sp^3 hybrid bonds of the C/Cu composite films are presented to reveal the physical mechanism by Raman spectroscopy.[24,28–30]

†Corresponding author. E-mail: zhaoyanan1984@xjtu.edu.cn
‡Corresponding author. E-mail: cuiwanzhao@126.com

© 2022 Chinese Physical Society and IOP Publishing Ltd

2. Experiment

Undoped carbon films and Cu films were deposited by a magnetron sputtering system at argon pressure of 1.5 Pa with microwave power at 150 W and 70 W, respectively. Cu-doped C films with different compositions were prepared by controlling the sputtering powers, as shown in Table 1. Two experimental samples of different sputtering systems were obtained finally. The amount of metal nanoparticles deposited on the surface of the film is different since the growth rates of C and Cu are different. Thus, it is evident that the surface colors of samples obtained by different preparation processes are quite different. The process parameters for the preparation of the C/Cu composite films are listed in Table 1.

Table 1. Preparation parameters of the Cu-doped carbon films.

Serial number	C/Power	Cu/Power	Time	n_{Cu}/n_C
/	MC/150 W	/	1 h	/
/	/	DC/70 W	40 min	/
A	MC/200 W	DC/15 W	1 h	0.135
C	MC/150 W	DC/15 W	1 h	0.173
D	MC/100 W	DC/15 W	1 h	0.204
B	MC/50 W	DC/15 W	1 h	0.226
E	MC/150 W	DC/35 W	1 h	0.245
F	MC/150 W	DC/55 W	1 h	0.452
G	MC/150 W	DC/75 W	1 h	0.645

3. Results

Firstly, we test the aluminum alloy substrate with pure Cu-plated surface using the SEY characteristic test platform, and the sample is with pure C-plated film. The test results are shown in Fig. 1(a). It can be obtained that the δ_{max} of the Ag-plated aluminum alloy substrate, the Cu-coated sample and the C-coated sample are 2.522, 1.920, and 1.362, respectively. It is found that the secondary electron yield coefficient (δ) of the substrate surface is significantly reduced after coating, and the δ of the sample with a Cu film sputtered on the surface is reduced by about 0.6 compared to the aluminum alloy substrate, which is about 23.79%. In addition, it can be obtained that the primary energy of the maximum (E_{max}, electronvolt) of the Cu-plated aluminum alloy substrate, Cu-plated sample, C-plated sample is 300 eV, 300 eV, 200 eV, respectively. The coating process can significantly control the SEY effect.

Secondly, the SEY curves of various C and Cu doping ratios are shown in Fig. 1(b). We can find that the Cu-doped and C-based nano-films can suppress the SEY. With the increase of the metal Cu doping ratio, the δ_{max} can be reduced from 1.69 to 1.53. The best suppression effect is the G sample with n_{Cu}/n_C of 0.645, and its δ_{max} is 1.53. Compared with the Ag-plated Al alloy substrate, its suppression effect is increased by 39.28%, and the suppression effect has been increased by 20.31% compared with the pure Cu sample. The poorer suppression effect is the sample E with an n_{Cu}/n_C of 0.245, and its δ_{max} is 1.69. Compared with the Ag-plated aluminum alloy substrate, the suppression effect is increased by 32.94%, and the suppression effect is increased by 11.98% compared with the pure Cu film. The suppression effect of the C/Cu composite film is poor, and the δ_{max} of all doped samples is higher than 1.36 compared with the pure C film. Based on the data in Fig. 1(a), the least squares polynomial fitting is used to fit the curve of δ_{max} with the C/Cu doping ratio, as shown in Fig. 1(c). The SEY coefficient shows a nonmonotonic relationship that increases at first and then decreases with the Cu doping contents.

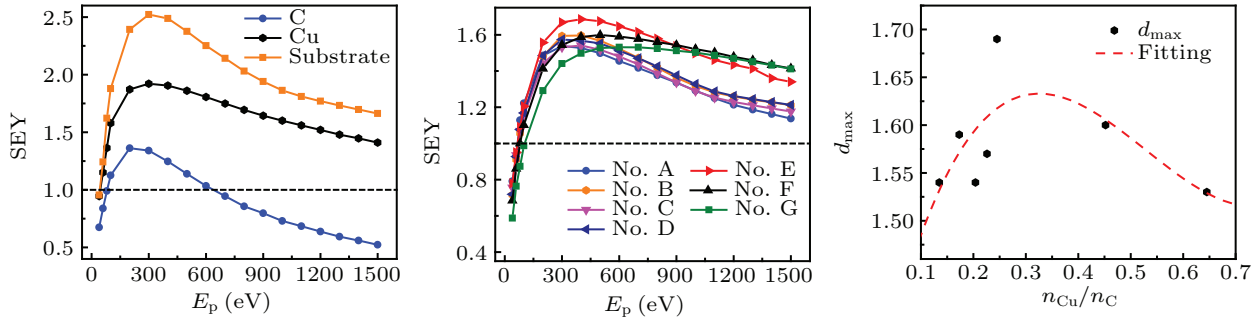


Fig. 1. (a) Secondary electron yield curves of aluminum alloy substrate with Ag plating, pure Cu-plated film sample and pure C-plated film sample. (b) The compared secondary electron yield curves of different doping C/Cu samples. (c) The δ_{max} of C/Cu composite film and its fitting trend curve.

The percentages of C and Cu of samples A–G are obtained by using an x-ray photoelectron spectroscopy, as shown in Fig. 2(a). All the samples show the C and Cu elements. Then, the corresponding ratios of n_C/n_{Cu} are obtained by peak fitting, as shown in Table 1.

In order to analyze the influence of the structure of the sample on the SEY, we use the field emission scanning electron microscopy (SEM) to characterize the surface and cross-sectional morphology of the B, C and G Cu-doped C-based nano-film samples, and the inset shows the corresponding sample. According to the sample morphology shown in Figs. 2(b), 2(c), 2(d), when the Cu doping ratio in the C-based composite film is small, such as B (n_{Cu}/n_C: 0.173) and C (n_{Cu}/n_C: 0.204) samples. The surface of the film sample is flat and the cross-sectional morphology is dense relatively. With the increase of the Cu doping ratio in the composite film, such

as sample G (n_{Cu}/n_C: 0.645), the size of the nano-particles on the surface of the film becomes larger and a large number of nano-particles are precipitated, obvious pores appear, and the surface morphology changes. It can be seen from the cross-sectional morphology that the compactness of the film becomes worse, forming a porous, loose and rough "coral-reef"-like structure.

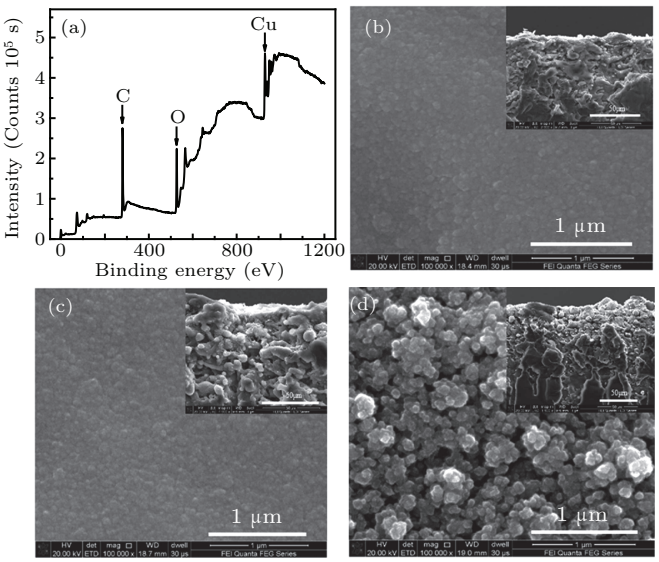


Fig. 2. (a) The XPS of the C/Cu composite films. Surface morphology of C/Cu composite films with different Cu contents. (b) Sample B n_{Cu}/n_C: 0.173. (c) Sample C n_{Cu}/n_C: 0.204. (d) Sample G n_{Cu}/n_C: 0.645.

The reasons for the above-mentioned changes in sample morphology seem to be that, on the one hand, the change of sputtering power during film growth not only affects the change of metal doping ratio, but also changes the energy and intensity of incident ions, thereby affecting the structure of the film. On the other hand, the surface of the film forms clusters with small scale and loose structure because there is no chemical bond between Cu and C atoms. The Cu nanoparticles in the film cause crystal lattice defects through dislocation slippage, etc., and then make up a series of "trap" structure. In addition, the Cu nanoparticles serve as a buffer material in the film, which can significantly reduce the internal stress and improve the film-base bonding force to a certain extent.

Since the samples F and G are seriously oxidized, Raman spectroscopy could not be obtained because of the obvious fluorescence interference. Therefore, Raman spectroscopy was performed on samples A–E, as shown in Fig. 3(a). The analysis of Raman spectroscopy is important to gain a better understanding how the Cu doping will affect sp^2 and sp^3 hybridization types of coordination bonds. Through the data processing method of peak fitting, the Raman spectra of samples A–E are analyzed, respectively. First, two different Gaussian peaks are obtained as shown by the red curve (D) near 1390 cm^{-1} and the green curve (G) near 1585 cm^{-1}. By sorting out the Raman data of samples A–E, the information such as the half width of the G peak is given in Table 3. It can be obtained that with the increase of the metal Cu doping ratio, I_D/I_G shows a monotonous decreasing trend, and the change trend of the peak position of the G peak is first increasing, then decreasing, and then increasing again, as shown in Fig. 3(b). G_{FWHM} is the overall increasing trend at the same time, which includes rise and fall alternating as shown in Fig. 3(c).

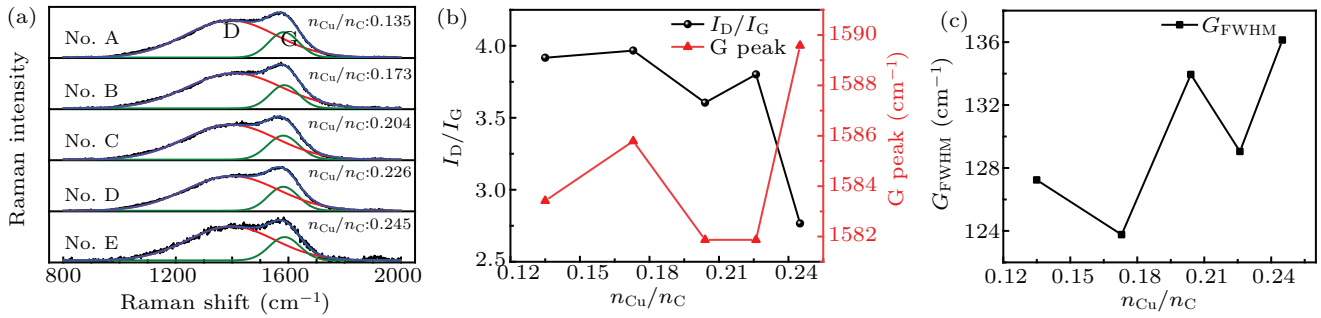


Fig. 3. (a) Raman spectrum of samples A–E. (b) The change trend of I_D/I_G and G peak position. (c) The change trend of G_{FWHM}.

Table 2. Raman spectroscopy analysis of the C/Cu composite samples.

Serial number	n_{Cu}/n_C	D peak (cm^{-1})	G peak (cm^{-1})	D_{FWHM} (cm^{-1})	G_{FWHM} (cm^{-1})	I_D/I_G
A	0.135	1394.67	1583.42	381.59	127.24	3.917
B	0.173	1408.86	1585.79	399.53	123.76	3.967
C	0.204	1396.25	1581.87	385.00	133.94	3.605
D	0.226	1399.41	1581.87	391.32	129.05	3.801
E	0.245	1397.83	1589.58	378.112	136.13	2.766
F	0.452	/	/	/	/	/
G	0.645	/	/	/	/	/

As can be seen from Fig. 3(b), with the change of doping ratio, I_D/I_G decreases from 3.917 to 2.766, a drop of 29.38%. The peak position of the G peak increases from 1583.42 cm^{-1} to 1589.58 cm^{-1}, and moves about 6 cm^{-1} to the high wave number range. The peak intensity ratio of the D peak to the G peak first decreases from 3.917 to 3.605 and then increases to 3.801 when the doping ratio is less than 0.245, a decrease of 2.96%; the peak position of the G peak first increases from 1583.42 cm^{-1} to 1585.79 cm^{-1} and then decreases to 1581.87 cm^{-1}, a decrease of about 0.98%, indicating that the sp^2 hybrid bond content in the C-based composite film is generally decreasing. As shown in Fig. 3(c), when the doping ratio is less than 0.245, the G_{FWHM} increases from 127.24 cm^{-1} to 129.05 cm^{-1}, the overall increase is 1.42%, and the degree of disorder of the film decreases, indicating that the sp^2 hybrid bond content of C-based composite film is reduced overall.[6] Comprehensive analysis of the reasons for the above phenomenon, firstly, the energy of the sputtered metal ions can be injected into the C film to promote the conversion of sp^2 bonds to sp^3 bonds, and result in increasing the content of sp^3 bonds in the film. However, as shown in Table 1, the sputtering power of Cu is 15 W for samples A, B, C, and D, which is not enough to damage the structure of the sp^3 hybrid bond. Secondly, the temperature of the film surface is not enough to promote the conversion of sp^3 bonds to sp^2 bonds in the film. Thirdly, more Cu nanoparticles may be precipitated after the sputtering process, since Cu has little solid solubility in the amorphous C network, such as sample F. Here, the sputtering power of Cu is 55 W and 75 W for samples F and G, respectively. Thus, there would exist more nanoparticles in the larger Cu doping samples.

Considering the above analysis, the mechanism can be summarized as follows: Firstly, according to the sample morphology, with the increase of Cu doping ratio, the size and number of the nanoparticles becomes larger on the surface of the film, and then obvious pores appear. It can be seen that the compactness of the film becomes worse, forming a porous, loose and rough "coral-reef"-like structure. Such a "trap" structure can effectively inhibit the secondary electron emission to some extent. Secondly, due to the small solid solubility of Cu in the amorphous carbon network, more Cu nanoparticles will be precipitated. Moreover, Cu is easy to be oxidized in the atmosphere. The generated metal oxide has a higher secondary electron emission coefficient. Thus, the inhibition effect of secondary electron emission is poor. Thirdly, the number of sp^2 hybrid bond decreases as the increase of the Cu doping ratio in the prepared films. The lower sp^2 content would lead to fewer free electrons, and the excited secondary electrons in the full band are less likely to collide with free electrons as they move toward the surface. Therefore, the escape ability is improved, and the suppression of SEY is reduced. The interaction of the three conditions makes the SEY coefficient increase first and then decrease.

4. Conclusion

In summary, various Cu-doped carbon films have been sputtered by controlling the sputtering power and the depositing time, and the mechanism of secondary electron suppression is analyzed. The lowest δ_{max} can reach 1.53 in the Cu doping sample (n_{Cu}/n_C, 0.645), and its suppression effect is increased by 39.28% compared with the Ag-plated Al alloy substrate. It is found that SEY increases with Cu contents due to the oxidation susceptibility of Cu and the decrease of sp^2 bonds. However, the addition of Cu increases the roughness and the number of charge traps of the carbon film, which efficiently reduces the SEY. Low SEY in Cu-doped carbon films deposited on Ag-plated aluminum alloy is potentially useful for applications in high power microwave components.

Acknowledgements

This work was supported by the National Key Laboratory Foundation (Grant Nos. 2018SSFNKLSMT-04,614241101010117 and 6142411191110) and the National 111 Project of China (Grant No. B14040).

References

[1] Xie A G, Xiao S R, Zhan Y and Zhao H F 2012 *Chin. Phys. Lett.* **29** 117901
[2] Xie A G, Zhang J and Wang T B 2011 *Chin. Phys. Lett.* **28** 097901
[3] Feng G B, Cui W Z, Zhang N, Cao M and Liu C L 2017 *Chin. Phys. B* **26** 097901
[4] Wang H, Cao L H, Zhao Z Q, Yu M Y, Gu Y Q and He X T 2014 *Chin. Phys. B* **23** 055202
[5] Montero I, Mohamed S H, Garcia M, Galan L and Raboso D 2007 *J. Appl. Phys.* **101** 113306
[6] Miao G, Cui W, Zhang N, Yang J and Zhang H 2016 *IEEE International Conference on High Voltage Engineering and Application (ICHVE)*
[7] Lu Q, Yu B, Hu Z, He Y, Hu T, Zhao Y, Wang Z, Zhou Z, Cui W and Liu M 2020 *Appl. Surf. Sci.* **501** 144236
[8] Ye M, Feng P, Wang D, Song B P, He Y N and Cui W Z 2019 *Chin. Phys. B* **28** 077901
[9] Yun L, Wanzhao C, Zhang H T, Yin X S, Wang H G, Jianfeng Z and He Y N 2017 *Chin. Space Sci. Technol.* **37** 73
[10] Dionne and Gerald F 1973 *J. Appl. Phys.* **44** 5361
[11] Dionne G F 1975 *J. Appl. Phys.* **46** 3347
[12] Wang X 2018 *J. Mech. Engin.* **54** 115
[13] Zhang W, Zhang X, Fang F and Jiang J 2009 *Chin. J. Vacuum Sci. Technol.* **29** 282
[14] Cui W Z, Li Y, Yang J, Hu T C, Wang X B, Wang R, Zhang N, Zhang H T and He Y N 2016 *Chin. Phys. B* **25** 068401
[15] Ye M, He Y N, Hu S G, Wang R, Hu T C, Yang J and Cui W Z 2013 *J. Appl. Phys.* **113** 124404
[16] Wang D, He Y and Cui W 2018 *Surf. Technol.* **47** 9
[17] Ma J, Wei L, Bai Y, Bao Y, Kang Q, Zhang W, Cui W, Hu T and Wu D 2021 *Thin Solid Films* **725** 138633
[18] Ye M, Ye Y, Wang R, Hu T, Zhang N, Yang J, Cui W and Zhang Z 2014 *Acta Phys. Sin.* **63** 147901 (in Chinese)

[19] Bai C J, Feng G B, Cui W Z, He Y N, Zhang W, Hu S G, Ye M, Hu T C, Huang G S and Wang Q 2018 *Acta Phys. Sin.* **67** 037902 (in Chinese)
[20] He Y, Yu B, Wang Q, Bai C, Yang J, Hu T, Xie B and Cui W 2018 *Acta Phys. Sin.* **67** 087901 (in Chinese)
[21] Robertson J F R 2002 *Mater. Sci. Engin. R* **37** 129
[22] Zhang Y X, Wang Y G, Wang S H, Wei W, Ge X Q, Zhu B L, Shao J Q and Wang Y 2020 *Coatings* **10** 884
[23] Aijaz A, Sarakinos K, Lundin D, Brenning N and Helmersson U 2012 *Diam. Relat. Mater.* **23** 1
[24] Ferrari A C and Robertson J 2004 *Philos. Trans. A Math. Phys. Eng.* **362** 2477
[25] Toh C T, Zhang H, Lin J, Mayorov A S, Wang Y P, Orofeo C M, Ferry D B, Andersen H, Kakenov N, Guo Z, Abidi I H, Sims H, Suenaga K, Pantelides S T and Ozyilmaz B 2020 *Nature* **577** 199
[26] Nguyen H K A, Mankowski J, Dickens J C, Neuber A A and Joshi R P 2018 *AIP Adv.* **8** 015325
[27] Guo Q and Zhang J 2013 *Guti Dianzixue Yanjiu Yu JinzhanResearch and Progress of Solid State Electronics* **33** 420 (in Chinese)
[28] Casiraghi C, Ferrari A C and Robertson J 2005 *Phys. Rev. B* **72** 085401
[29] Ferrari A and Robertson J 2000 *Phys. Rev. B* **61** 14095
[30] Caro M A, Deringer V L, Koskinen J, Laurila T and Csanyi G 2018 *Phys. Rev. Lett.* **120** 166101